

Review

The Application of Nano Titanium Dioxide for Hydrogen Production and Storage Enhancement

Angelantonio De Benedetto¹, Agnese De Luca¹, Paolo Pellegrino^{1,2} , Rosaria Rinaldi^{1,2} ,
Valeria De Matteis^{1,2,*}  and Mariafrancesca Cascione^{1,2,*} 

¹ Department of Mathematics and Physics “E. De Giorgi”, University of Salento, Via Monteroni, 73100 Lecce, Italy; angelantonio.debenedetto@unisalento.it (A.D.B.); agnese.deluca@unisalento.it (A.D.L.); paolopellegrino@unisalento.it (P.P.); ross.rinaldi@unisalento.it (R.R.)

² Institute for Microelectronics and Microsystems (IMM), National Research Council (CNR), Via Monteroni, 73100 Lecce, Italy

* Correspondence: valeria.dematteis@unisalento.it (V.D.M.); mariafrancesca.cascione@unisalento.it (M.C.)

† These authors contributed equally to this work.

Abstract: The utilization of hydrogen (H₂) as a renewable and clean energy carrier, free from the reliance on fossil fuels, represents a significant technological challenge. The use of renewable energy sources for hydrogen production, such as photocatalytic hydrogen generation from water under solar radiation, has garnered significant interest. Indeed, the storage of hydrogen presents another hurdle to the ongoing advancement of hydrogen energy. Concerning solid-state hydrogen storage, magnesium hydride (MgH₂) has emerged as a promising option due to its high capacity, excellent reversibility, and cost-effectiveness. Nevertheless, its storage performance needs improvement to make it suitable for practical applications. Titanium dioxide (TiO₂) has distinguished itself as the most extensively researched photocatalyst owing to its high photo-activity, good chemical and thermal stability, low toxicity, and affordability. This review highlights the application of TiO₂ for hydrogen production under visible and solar light, with a particular focus both on its modification without the use of noble metals and its utilization as a catalyst to enhance the hydrogen storage performance of MgH₂.

Keywords: titanium dioxide; hydrogen production; hydrogen storage



Citation: De Benedetto, A.; De Luca, A.; Pellegrino, P.; Rinaldi, R.; De Matteis, V.; Cascione, M. The Application of Nano Titanium Dioxide for Hydrogen Production and Storage Enhancement. *Appl. Sci.* **2023**, *13*, 12521. <https://doi.org/10.3390/app132212521>

Academic Editors: Hicham Idriss and Leonarda Liotta

Received: 13 October 2023

Revised: 14 November 2023

Accepted: 15 November 2023

Published: 20 November 2023



Copyright: © 2023 by the authors. Licensee MDPI, Basel, Switzerland. This article is an open access article distributed under the terms and conditions of the Creative Commons Attribution (CC BY) license (<https://creativecommons.org/licenses/by/4.0/>).

1. Introduction

The extensive consumption of fossil fuels, particularly over the past century, has significantly contributed to environmental pollution. As environmental and socio-economic consciousness continues to grow, governments and legislative bodies worldwide are expressing concern and examining the factors associated with pollution that affect the energy landscape. Consequently, there is an urgent requirement to replace fossil fuels with renewable, eco-friendly, and alternative energy sources [1–5].

Therefore, to date, the most pressing scientific and technological challenge is the development of a renewable and clean energy that does not rely on fossil fuels. From this perspective, one of the most appealing options for large-scale utilization is hydrogen as a recyclable energy carrier. Consequently, green approaches to hydrogen production, such as the photocatalytic process from water under solar radiation, has garnered considerable interest [6,7]. For photocatalytic hydrogen production, titanium dioxide (TiO₂) represents a promising candidate among various inorganic semiconductor photocatalysts [8,9] due to its high efficiency, high stability, non-toxicity, and low cost. However, the practical application remains constrained, since TiO₂ responds solely to ultraviolet light, which constitutes approximately 4% of the solar spectrum. Therefore, it is mandatory to design and synthesize TiO₂-based photocatalytic systems capable of reacting to the whole visible light range, accounting for ~43% of the solar spectrum, thus improving the efficiency [10,11].

The storage of hydrogen to provide grid energy from intermittent energy sources is another major challenge for the further development of hydrogen energy [12]. On the other hand, magnesium hydride (MgH₂) stands out as one of the most promising candidates in solid-state hydrogen storage thanks to its high capacity (7.6 wt%), excellent reversibility, and cost-effectiveness. Nonetheless, its practical application is constrained by its high operating temperature requirements and suboptimal kinetic performance [13]. An effective approach to enhance the hydrogen storage performance of MgH₂ involves the introduction of catalysts, which may encompass metals [14–16], metal oxides [16–19], metal sulfides [20,21], and metal halides [19,22].

Focusing on work published in the last decade, this review firstly delves into the utilization of TiO₂ for hydrogen production under visible and solar light, as well as its role in enhancing the hydrogen storage performance of MgH₂. Successively, in the domain of hydrogen production, various strategies aimed at enhancing TiO₂ performance without the use of noble metals are explored.

2. Titanium Dioxide

TiO₂ is the most widely investigated photocatalyst due to its remarkable photo-activity, strong chemical and thermal stability, low toxicity, and cost-effectiveness [23]. In nature, four polymorphs of TiO₂ are found: anatase (tetragonal), rutile (tetragonal), brookite (orthorhombic), and TiO₂(B) (monoclinic). Additionally, two high-pressure forms have been synthesized starting from rutile: TiO₂(II) and TiO₂(H) [24]. However, rutile and anatase are indeed the two most common crystalline forms of TiO₂, and they find numerous applications owing to their unique properties [25]. TiO₂ is an n-type semiconductor, and for bulk materials, anatase has a band gap of 3.20 eV, which corresponds to an absorption threshold at a wavelength of 384 nm, while rutile has a band gap of 3.02 eV, which corresponds to an absorption threshold at the 410 nm wavelength [24]. Therefore, near-ultraviolet (UV) radiation is necessary to excite anatase, whereas the photo-response of rutile slightly extends into the visible light spectrum [26]. These varying band gap values can be attributed to differences in the lattice structures of anatase and rutile TiO₂, resulting in distinct densities and electronic band structures [24]. The TiO₂ photocatalytic activity depends on several factors, including phase structure, specific surface areas, crystallite size, and pore structure. Moreover, the photocatalytic activity of anatase is generally considerably higher than that of rutile [27]. The absorption of photons with energy equal to or greater than the band gap results in the generation of electron–hole pairs through the excitation of electrons from the valence band to the conduction band of the semiconductor. When both electrons and holes migrate to the surface of semiconductor without recombination, the photogenerated electrons can participate in reduction reactions, while the holes engage in oxidation reactions. These processes form the basis for photocatalytic water splitting and the photodegradation of organic pollutants [28].

2.1. Hydrogen Production Exploiting TiO₂ under Visible and Solar Light

Water splitting is an uphill reaction that needs the standard Gibbs free energy change of 237 kJ mol^{−1} [2]. It consists of two half reactions [3]:



Therefore, the overall reaction is [2]:



In order for a semiconductor to function as a photocatalyst for water splitting, it is imperative that the bottom of its conduction band exhibits a more negative potential than the reduction potential of H⁺/H₂ at 0 V versus the normal hydrogen electrode (NHE).

Simultaneously, the top of its valence band should possess a more positive potential than the oxidation potential of O_2/H_2O at 1.23 V versus NHE. Therefore, for efficient water splitting, the band gap of the semiconductor should exceed 1.23 eV; conversely, to harness visible light, the band gap should be less than 3.0 eV [29]. Accordingly, a band gap falling within the range of (1.23–3.0) eV is a necessary requisite. In addition, photocatalytic H_2 generation is influenced by some factors such as surface area and particle size, band gap energy, corrosion resistance, and the presence of a sacrificial agent [3] such as glycerol [1], triethanolamine (TEOA) [10], ethanol [30], or methanol [11].

For H_2 production, the performance of TiO_2 is generally limited by the high recombination rate of the photogenerated electrons and holes, an inability to utilize visible light, and fast backward reactions [31]. Loading TiO_2 with noble metals such as Pt, Au [32–34], or Pd [35] allows the photocatalytic efficiency of TiO_2 to be enhanced by reducing the fast recombination of photogenerated charge carriers [11] and allows the TiO_2 response to the entire visible light spectral range to be extended [3]. However, the use of noble metals is expensive, and their availability is limited; consequently, their use is unsuitable for large-scale energy production [11]. For these reasons, other strategies have been optimized to improve the photocatalytic efficiency of TiO_2 , such as employing non-noble metals, metal oxides, cadmium sulfide (CdS), and molybdenum disulfide (MoS_2).

Below, different TiO_2 modification strategies that have been evaluated under visible and solar light are presented.

2.1.1. Modification of TiO_2 with Non-Noble Metals and Metallic Oxides

Numerous approaches have been developed to improve the photocatalytic response of TiO_2 , in terms of both broadening the reaction spectrum to the entire visible spectral range [11] and mitigating the rapid recombination phenomena of electron–lacuna pairs [36].

The incorporation of non-noble metals (such as Fe, Cu, Co, Ni, and Cr) or metallic oxides onto TiO_2 represents a valid alternative to noble metals. In particular, the use of this approach can effectively hinder the recombination of electron–hole pairs and promote the separation of charge carriers [37].

Subha et al. [38] synthesized a photocatalyst system based on TiO_2 doped with Cu and Zn ($CuZn-TiO_2$). TEM images and XPS spectra showed the presence of Cu_2O , CuO , ZnO , and Cu^0 on the TiO_2 surface. Metal–semiconductor junctions and heterojunctions between semiconductors were formed due to the growth of Cu_2O , CuO , ZnO , and Cu^0 on the surface of TiO_2 . Effective charge separation due to the heterojunctions and high electron mobility due to Cu^0 improved the H_2 production. In addition, Cu^0 , CuO , and Cu_2O allowed the absorption of TiO_2 to shift to visible light. In particular, the $CuZn-TiO_2$ with an optimum loading of Cu and Zn of 0.5 wt% achieved a H_2 production of about $14,521 \mu\text{mol h}^{-1} \text{g}^{-1}_{\text{cat}}$ under solar light, using glycerol as sacrificial reagent. A plausible mechanism for H_2 production is reported in the work of Subha et al. [38] and is schematically represented in Figure 1.

A cobalt (Co)-doped TiO_2 photocatalyst was synthesized by Sadanandam et al. [36] through the impregnation method. The presence of cobalt species on the TiO_2 surface of the synthesized photocatalyst was observed. The Co/TiO_2 photocatalyst, with 1 wt% of Co doped on TiO_2 P25, achieved a maximum hydrogen production of $11,021 \mu\text{mol h}^{-1} \text{g}^{-1}$ from aqueous glycerol solutions under solar light irradiation, showing that Co^{2+} ions can extend the photo-response of TiO_2 into the visible region [36].

Díaz et al. [11] prepared a series of photocatalyst systems consisting of TiO_2 P25 combined with Fe, Co, Ni, Cu, and Zn (denoted as Fe/TiO_2 , Co/TiO_2 , Ni/TiO_2 , Cu/TiO_2 , and Zn/TiO_2 , respectively) using the impregnation method. The TiO_2 was loaded with 2 wt% of the selected transition metal and evaluated under both visible and UV light irradiation. During visible light exposure, with methanol serving as a sacrificial reagent, the photocatalysts Ni/TiO_2 , Co/TiO_2 , Zn/TiO_2 , and Fe/TiO_2 exhibited lower H_2 production rates than the pure TiO_2 . Conversely, Cu/TiO_2 demonstrated a substantial enhancement in photocatalytic activity, yielding H_2 production rates equal to $220 \mu\text{mol h}^{-1} \text{g}^{-1}$ [11].

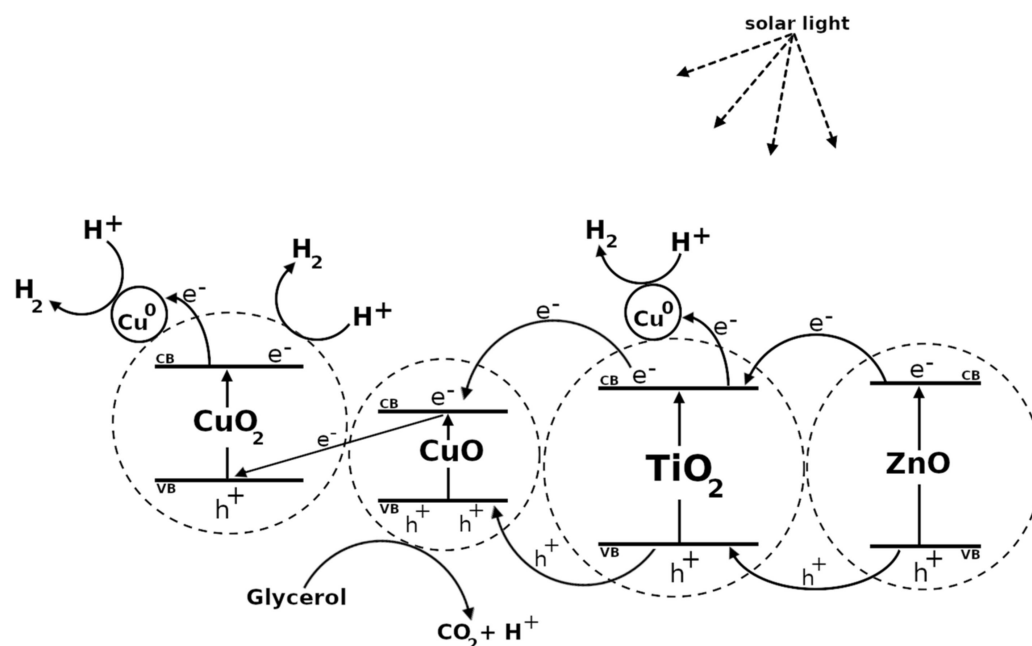


Figure 1. Schematic representation of a possible mechanism (Z-scheme mechanism with double charge transfer mechanism) for H₂ production by CuZn-TiO₂ photocatalyst under solar light.

Kotesh Kumar et al. [39] developed a photocatalyst system comprising bimetallic Cu-Ni alloy NPs decorated on TiO₂ P25. The Cu-Ni/TiO₂ photocatalyst, with a Cu loading of 2 mol% and Ni loading of 5 mol%, achieved a remarkable H₂ evolution rate of 35.4 mmol g⁻¹ h⁻¹ under solar light conditions, employing methanol as a sacrificial reagent. Additionally, the monometallic photocatalysts Cu-doped TiO₂ (Cu/TiO₂) and Ni-doped TiO₂ (Ni/TiO₂) were also synthesized and assessed. It was observed that the monometallic photocatalysts exhibited lower H₂ yields compared to the Cu-Ni/TiO₂ systems [39]. Reddy et al. [40] fabricated mesoporous nano TiO₂ and introduced Fe/TiO₂ catalysts by synthesizing and introducing Fe dopants onto the TiO₂ surface through the impregnation process. These catalysts were tested under solar light irradiation and the H₂ production rate of 270 μmol/h was attained with 0.5 wt% of Fe³⁺ loading. A comparison between Fe doping on the TiO₂ surface and Fe doping into the TiO₂ lattice revealed that metal ions should be doped in the proximity to the TiO₂ surface to achieve efficient photocatalytic activity through enhanced charge transfer [40]. Police et al. [1] prepared a Cu₂O/TiO₂/Bi₂O₃ ternary photocatalyst: the presence of Cu₂O and Bi₂O₃ allows the visible-light absorption to be extended and helps minimize the electron–hole recombination of TiO₂, respectively. When exposed to solar light irradiation, the ternary photocatalyst, with 2 wt% Cu and 2 wt% Bi, demonstrated an impressive H₂ production rate of 3678 μmol/h in glycerol aqueous solution. Furthermore, the dependence of photocatalytic H₂ production on the glycerol and catalyst content was investigated. It was observed that under an optimal glycerol concentration and catalyst amount, a H₂ production rate of 6727 μmol/h was achieved [1].

A photocatalyst consisting of mesoporous ZrO₂-TiO₂ NPss anchored on reduced graphene oxide (rGO) was synthesized by Subha et al. [41]. The ZrO₂-TiO₂/rGO photocatalyst, with a loading of 1.0 wt% of ZrO₂ and rGO on TiO₂, exhibited remarkable H₂ production (~7773 μmol h⁻¹ g⁻¹) in a glycerol aqueous solution under solar light irradiation. Furthermore, a ZrO₂-TiO₂ photocatalyst, with 1.0 wt% of ZrO₂ loading on TiO₂, was also examined, and it achieved an H₂ production rate of 5781 μmol h⁻¹ g⁻¹. The ZrO₂-TiO₂ heterojunction anchored on rGO sheets demonstrated the suppression of electron–hole pair recombination and an enhancement in the efficiency of interfacial charge transfer [41].

Praveen Kumar et al. [42] synthesized a photocatalyst composed of CuO deposited onto TiO₂ nanotubes. The photocatalyst, with a copper loading of 1.5 wt%, exhibited

the highest photocatalytic hydrogen evolution rate under solar light using glycerol as a sacrificial agent. It achieved an impressive H_2 production rate of $99,823 \mu\text{mol h}^{-1} \text{g}^{-1}$ [42].

Subha et al. [43] synthesized a $\text{Cu}_x\text{O}/\text{TiO}_2$ nanocomposite loaded with layered $\text{Ni}(\text{OH})_2$. Under solar light irradiation and in the presence of glycerol (5 vol%), the $\text{Ni}(\text{OH})_2$ - $\text{Cu}_x\text{O}/\text{TiO}_2$ photocatalyst, with an optimal loading of 1.0 wt% $\text{Ni}(\text{OH})_2$ and 0.5 wt% Cu_xO , showed a H_2 production of $\sim 15,789 \mu\text{mol h}^{-1} \text{g}^{-1}$. Furthermore, Cu-doped TiO_2 photocatalysts ($\text{Cu}_x\text{O}/\text{TiO}_2$) were tested. It was shown that the photocatalyst with 0.5 wt% Cu loading on TiO_2 allowed an advancement in H_2 production ($\sim 7679 \mu\text{mol h}^{-1} \text{g}^{-1}$) [43].

2.1.2. Coupling TiO_2 with CdS

The CdS semiconductor has been extensively studied as a sensitizer for photocatalytic water splitting due to its narrow band gap and strong absorption in the visible-light spectral region [44]. Combining TiO_2 with a CdS semiconductor can further enhance the photocatalytic performance of TiO_2 [45]. Luo et al. [46] synthesized a CdS/ $\text{TiO}_2(\text{B})$ type II heterojunction via photo deposition, with CdS dots anchored on $\text{TiO}_2(\text{B})$ nanosheets. Under visible light, a H_2 evolution rate of $1577 \mu\text{mol g}^{-1} \text{h}^{-1}$ was achieved. Additionally, a CdS/ $\text{TiO}_2(\text{B})$ type I heterojunction was synthesized via the hydrothermal method; however, it resulted in a H_2 evolution rate of $48 \mu\text{mol g}^{-1} \text{h}^{-1}$ under visible light, significantly lower than that obtained with the type II heterojunction. The proposed mechanism for H_2 production by CdS/ $\text{TiO}_2(\text{B})$ reported by Luo et al. [46] is schematically represented in Figure 2.

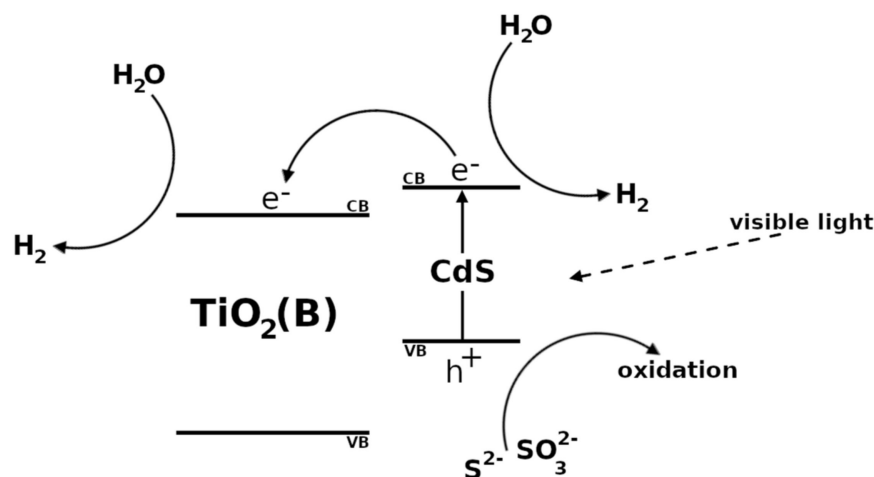


Figure 2. Schematic representation of a possible mechanism for H_2 production by CdS/ $\text{TiO}_2(\text{B})$ photocatalyst under visible light.

Zhu et al. [47] utilized TiO_2 nanotube arrays, obtained by anodizing titanium foils, in conjunction with CdS quantum dots to create CdS quantum dots decorated TiO_2 nanotube arrays. Under visible light and in the presence of Na_2SO_3 and Na_2S as sacrificial reagents, a H_2 production rate of $1.89 \mu\text{mol h}^{-1} \text{cm}^{-2}$ was achieved [47].

Gao et al. [44] prepared TiO_2 microspheres with highly exposed (001) facets loaded with CdS. They observed that CdS/ TiO_2 microsphere composites with a CdS: TiO_2 molar ratio of 1 indicated the highest activity, resulting in a H_2 production rate of $76.55 \mu\text{mol/h}$ when lactic acid was used as the scavenger for photo-generated holes under visible light [44].

A porous TiO_2 co-doped with CdS and WO_3 was synthesized by Qian et al. [45]. The ternary porous CdS/ WO_3/TiO_2 photocatalyst, with a molar ratio of CdS: WO_3 : TiO_2 equal to 8:8:100, achieved a H_2 evolution rate of $2106 \mu\text{mol g}^{-1} \text{h}^{-1}$ under visible light using Na_2S and Na_2SO_3 .

Furthermore, the binary CdS/ TiO_2 and WO_3/TiO_2 porous photocatalysts were tested, resulting in a H_2 evolution rate of $1056 \mu\text{mol g}^{-1} \text{h}^{-1}$ and $981 \mu\text{mol g}^{-1} \text{h}^{-1}$ for CdS/ TiO_2

and WO_3/TiO_2 , respectively. The possible mechanism for H_2 production using the $\text{CdS}/\text{WO}_3/\text{TiO}_2$ photocatalyst proposed by Qian et al. [45] is schematically represented in Figure 3.

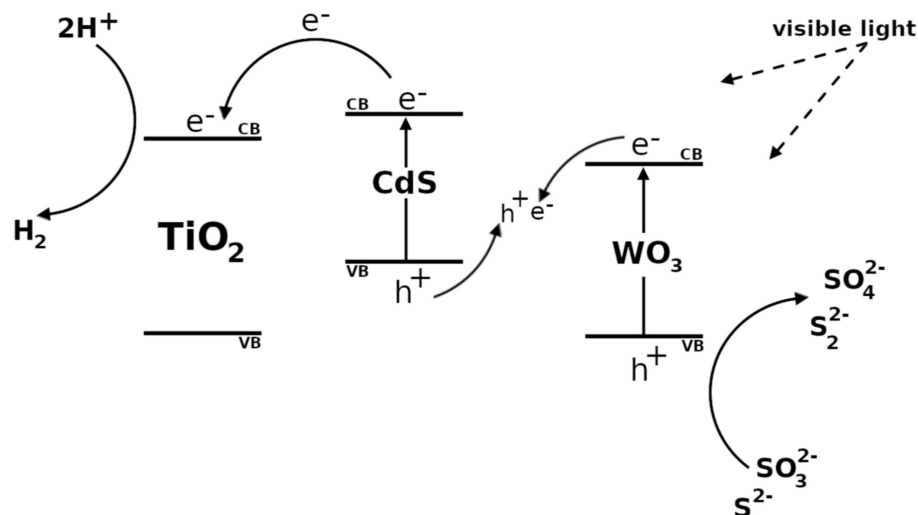


Figure 3. Schematic representation of a possible mechanism for H_2 production using the $\text{CdS}/\text{WO}_3/\text{TiO}_2$ photocatalyst under visible light.

2.1.3. Coupling TiO_2 with MoS_2

The efficiency of photocatalytic hydrogen production can also be improved by exploiting MoS_2 as a co-catalyst for TiO_2 [48]. Several strategies have been developed to improve the performance of $\text{MoS}_2/\text{TiO}_2$ photocatalysts under visible light. Yuan et al. [49] introduced a composite photocatalyst system based on TiO_2 nanosheets and MoS_2 , in which the visible light absorption of $\text{TiO}_2/\text{MoS}_2$ was expanded by incorporating CuInS_2 quantum dots as a light-harvesting inorganic dye. The ternary $\text{CuInS}_2/\text{TiO}_2/\text{MoS}_2$ photocatalyst with 0.6 mmol g^{-1} of CuInS_2 and 0.5 wt\% of MoS_2 exhibited a H_2 evolution rate of $1034 \mu\text{mol h}^{-1} \text{ g}^{-1}$ under visible light in the presence of Na_2S and Na_2SO_3 as sacrificial reagents. A possible mechanism for H_2 production is reported in the work of Yuan et al. [49] and is schematically represented in Figure 4. A Zn(II)-5,10,15,20-tetrakis(4-carboxyphenyl)-porphyrin (ZnTCPP)-sensitized $\text{MoS}_2/\text{TiO}_2$ photocatalyst was synthesized by Yuan et al. [10], exploiting the ZnTCPP to improve the absorption in visible light and the MoS_2 to enhance the photocatalytic activity. The ZnTCPP- $\text{MoS}_2/\text{TiO}_2$ photocatalyst was prepared by synthesizing $\text{MoS}_2/\text{TiO}_2$ composites, and then adsorbing the ZnTCPP dye on the TiO_2 surface. TiO_2 P25 was used. A H_2 production rate of $10.2 \mu\text{mol h}^{-1}$, under visible light, was achieved using the photocatalyst loaded with 1.00 wt\% of MoS_2 . TEOA was used as the sacrificial electron donor in the photocatalytic hydrogen evolution experiments. Shen et al. [50] synthesized MoS_2 nanosheet-porous TiO_2 nanowire hybrid nanostructures using the hydrothermal method. A H_2 evolution rate of $16.7 \text{ mmol h}^{-1} \text{ g}^{-1}$ was achieved under visible light in the presence of Eosin Y dye in TEOA aqueous solution. Flower-like $\text{MoS}_2@\text{TiO}_2$ catalysts were synthesized by Ma et al. [51] using a hydrothermal method, using a metal-organic framework (MOF) as a precursor. The $\text{MoS}_2@\text{TiO}_2$ photocatalysts, with a loading of 14.6 wt\% of MoS_2 , allowed a H_2 production rate of $10,046 \mu\text{mol h}^{-1} \text{ g}^{-1}$ under visible light to be achieved in the presence of fluorescein as photosensitizer in an aqueous acetone solution and using TEOA as a sacrificial donor.

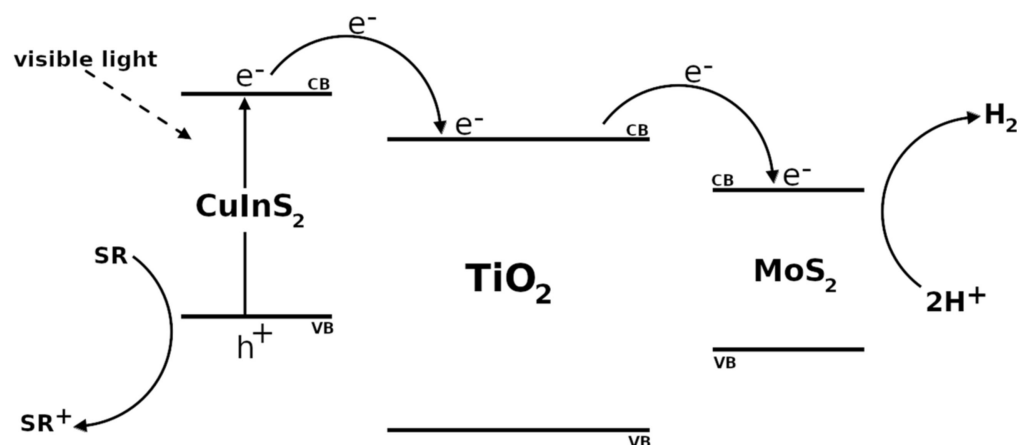


Figure 4. Schematic representation of a plausible mechanism for H_2 production by $CuInS_2/TiO_2/MoS_2$ photocatalyst under visible light.

2.1.4. Coupling TiO_2 with MoS_2 and CdS

Du et al. [52] developed a photocatalyst based on a porous TiO_2 monolith with MoS_2 nanosheets and CdS nanoparticles grown on the porous TiO_2 . The MoS_2 - CdS - TiO_2 photocatalyst was designed to exploit both CdS and MoS_2 to extend the absorption to visible light and to improve the hydrogen production efficiency. The MoS_2 - CdS - TiO_2 photocatalyst with 3% of MoS_2 and 10% of CdS (molar ratio to TiO_2) showed a H_2 generation rate of $4146 \mu\text{mol h}^{-1} \text{g}^{-1}$ using Na_2S and Na_2SO_3 as sacrificial reagents under visible light. In addition, CdS - TiO_2 and MoS_2 - TiO_2 photocatalysts were also tested. A H_2 generation rate of $875 \mu\text{mol h}^{-1} \text{g}^{-1}$ and $1360 \mu\text{mol h}^{-1} \text{g}^{-1}$ was obtained with CdS - TiO_2 and MoS_2 - TiO_2 , respectively. Qin et al. [53] prepared MoS_2/CdS - TiO_2 nanofibers via an electrospinning-mediated photo-deposition method. The MoS_2/CdS - TiO_2 photocatalyst, with a loading of 1 wt% of MoS_2 , showed a H_2 evolution rate of $280.0 \mu\text{mol h}^{-1}$ in a lactic acid aqueous solution under visible light.

The main works that describes TiO_2 -based photocatalysts modified with non-noble metals, metallic oxides, CdS , and MoS_2 for H_2 production under visible and solar light were summarized in Table 1.

2.2. Exploiting the TiO_2 Properties for Hydrogen Storage

For solid-state hydrogen storage, several materials such as MgH_2 [13,54–56], $NaAlH_4$ [57], $LiAlH_4$ [58], and $LiBH_4$ [59,60] have been considered due to their higher gravimetric and volumetric hydrogen densities [61]. However, their practical applications are limited due to their sluggish kinetic and high dehydrogenation temperature [54,57,58,62]. Concerning MgH_2 [13,54–56,63–68], $NaAlH_4$ [57,69,70], $LiAlH_4$ [71,72] and $LiBH_4$ [60,62], the use of TiO_2 as a catalyst has been investigated in order to improve the dehydrogenation/rehydrogenation kinetics of these materials, showing an improvement in performance by adding TiO_2 . Moreover, the use of TiO_2 has also been investigated for MgH_2 - $NaAlH_4$ composite [61] and $4MgH_2$ - $LiAlH_4$ composite [73]. Both composites showed significant improvements in the dehydrogenation/rehydrogenation kinetics with the introduction of TiO_2 .

Table 1. TiO₂-based photocatalysts modified with non-noble metals, metallic oxides, CdS, and MoS₂ for H₂ production under visible and solar light.

Photocatalyst	Crystalline Phases of TiO ₂	Loading	Irradiation	Sacrificial Reagents	H ₂ Production	Ref.
Cu ₂ O/TiO ₂ /Bi ₂ O ₃	anatase	2 wt% of Cu 2 wt% of Bi	solar light	glycerol	6727 μmol h ⁻¹	[1]
ZnTCPP-MoS ₂ /TiO ₂	anatase/rutile	1.00 wt% of MoS ₂	visible light	TEOA	10.2 μmol h ⁻¹	[10]
Cu/TiO ₂	anatase/rutile	2 wt% of Cu	visible light	methanol	220 μmol h ⁻¹ g ⁻¹	[11]
Co/TiO ₂	anatase/rutile	1 wt% of Co	solar light	glycerol	11,021 μmol h ⁻¹ g ⁻¹	[36]
CuZn-TiO ₂	anatase	0.5 wt% of Cu 0.5 wt% of Zn	solar light	glycerol	14,521 μmol h ⁻¹ g ⁻¹	[38]
Cu-Ni/TiO ₂	anatase/rutile	2 mol% of Cu 5 mol% of Ni	solar light	methanol	35.4 mmol h ⁻¹ g ⁻¹	[39]
Fe/TiO ₂	anatase	0.5 wt% of Fe ³⁺	solar light	-	270 μmol h ⁻¹	[40]
ZrO ₂ -TiO ₂ /rGO	anatase	1.0 wt% of ZrO ₂ 1.0 wt% of rGO	solar light	glycerol	7773 μmol h ⁻¹ g ⁻¹	[41]
CuO/TiO ₂	anatase/rutile	1.5 wt% of Cu	solar light	glycerol	99,823 μmol h ⁻¹ g ⁻¹	[42]
Ni(OH) ₂ -Cu _x O-TiO ₂	anatase	1.0 wt% of Ni(OH) ₂ 0.5 wt% of Cu _x O	solar light	glycerol	7679 μmol h ⁻¹ g ⁻¹	[43]
CdS/TiO ₂	anatase	CdS:TiO ₂ molar ratio of 1	visible light	lactic acid	76.55 μmol h ⁻¹	[44]
CdS/WO ₃ /TiO ₂	anatase	molar ratio 8:8:100	visible light	Na ₂ S and Na ₂ SO ₃	2106 μmol h ⁻¹ g ⁻¹ 1056 μmol h ⁻¹ g ⁻¹ 981 μmol h ⁻¹ g ⁻¹	[45]
CdS/TiO ₂ (B)	TiO ₂ (B)	5% of CdS	visible light	Na ₂ S and Na ₂ SO ₃	1577 μmol h ⁻¹ g ⁻¹	[46]
CdS/TiO ₂	anatase	-	visible light	Na ₂ S and Na ₂ SO ₃	1.89 μmol h ⁻¹ cm ⁻²	[47]
CuInS ₂ /TiO ₂ /MoS ₂	anatase	0.5 wt% of MoS ₂	visible light	Na ₂ S and Na ₂ SO ₃	1034 μmol h ⁻¹ g ⁻¹	[49]
MoS ₂ /TiO ₂ nanowire and Eosin Y	anatase	-	visible light	TEOA	16.7 mmol h ⁻¹ g ⁻¹	[50]
Flower-like MoS ₂ @TiO ₂ and fluorescein	anatase	14.6 wt% of MoS ₂	visible light	TEOA	10,046 μmol h ⁻¹ g ⁻¹	[51]
MoS ₂ -CdS-TiO ₂	anatase	3% of MoS ₂ and 10% of CdS molar ratio to TiO ₂	visible light	Na ₂ S and Na ₂ SO ₃	4146 μmol h ⁻¹ g ⁻¹	[52]
CdS-TiO ₂ MoS ₂ -TiO ₂		- -			875 μmol h ⁻¹ g ⁻¹ 1360 μmol h ⁻¹ g ⁻¹	
MoS ₂ /CdS-TiO ₂ nanofibers	anatase	1 wt% of MoS ₂	visible light	lactic acid	280.0 μmol h ⁻¹	[53]

Application of TiO₂ to Enhance the Hydrogen Storage Performance of MgH₂

Several strategies have been adopted to improve the hydrogen storage performance of MgH₂ by exploiting TiO₂ as catalyst. A carbon-supported nanocrystalline TiO₂ was synthesized by Zhang et al. [63] as a catalyst precursor. The carbon-supported nanocrystalline TiO₂ (TiO₂@C) exhibited good catalytic activity in the hydrogen storage reaction of MgH₂. It was observed that the TiO₂@C-containing MgH₂ composite with a TiO₂@C content of 10 wt% released 6.5 wt% hydrogen within 7 min at 300 °C. Moreover, the dehydrogenated sample took up approximately 6.6 wt% hydrogen within 10 min at 140 °C under 50 bar of H₂. Chen et al. [54] explored the catalytic effect of synthesized Co/TiO₂ nanocomposite on the hydrogen desorption/absorption properties of MgH₂. It was observed that using Co/TiO₂ highly improved the hydrogen desorption/absorption kinetics of MgH₂

in comparison to using Co or TiO₂ separately. The MgH₂-Co/TiO₂ composite showed an absorption of 6.07 wt% H₂ within 10 min at 165 °C under 60 bar of H₂ pressure and a dehydrogenation peak temperature of 235.2 °C. A sandwich-like structure composed of Ti₃C₂ and carbon-supported anatase TiO₂ (Ti₃C₂/TiO₂(A)-C) was developed by Gao et al. [55] in order to exploit the laminar MXene and the corresponding metal oxide to enhance the hydrogen absorption and desorption kinetics of MgH₂. The Ti₃C₂/TiO₂(A)-C structure was prepared using a heat treatment. The catalyst-doped MgH₂ composites with 5 wt% of Ti₃C₂/TiO₂(A)-C released approximately 5 wt% hydrogen within 1700 s at 250 °C under 0.05 MPa of hydrogen pressure, with a larger rate constant of 0.258 wt% min⁻¹. An uptake of approximately 4 wt% hydrogen within 800 s at 125 °C, under 3 MPa hydrogen pressure, was also observed. Unlike the preparation of the TiO₂/MXene heterostructure via the heat treatment of MXene, Gao et al. [13] also developed self-assembled TiO₂/Ti₃C₂T_x heterostructures through a one-step ultrasonic method at room temperature. The TiO₂ nanoparticles were self-assembled onto a few layers of Ti₃C₂T_x. The TiO₂/Ti₃C₂T_x-MgH₂ composite with 5 wt% of TiO₂/Ti₃C₂T_x achieved the fastest dehydrogenation and hydrogenation kinetics, showing a hydrogen desorption of 5.98 wt% within 600 s at 300 °C and a hydrogen absorption of 5.90 wt% within 1200 s at 175 °C. A catalyst composed of TiO₂ nanoparticles deposited on the pore wall of a three-dimensionally ordered macroporous (3DOM) structure was synthesized by Shao et al. [56]. It was observed that the 3DOM TiO₂ catalyst improved the hydrogen storage properties of MgH₂. The MgH₂-3DOM TiO₂ composite showed a hydrogen desorption of 5.75 wt% within 1000 s at 300 °C. A hydrogen absorption of 4.17 wt% within 1800 s even at 100 °C was observed. Jardim et al. [64] investigated the effects of TiO₂ nanorods on the absorption/desorption properties of MgH₂. The TiO₂ nanorods were produced through titanate nanotube heat treatment, whereas titanate nanotubes were synthesized via the alkaline hydrothermal route using commercial TiO₂ anatase as a starting material. At 350 °C, the MgH₂-TiO₂ nanorod composite showed a hydrogen absorption of 5.5 wt% after 10 min under 10 bar of hydrogen pressure. Furthermore, it was observed that after 5 min at 350 °C under 0.1 bar of hydrogen pressure, the composite desorbed around 100% of the absorbed hydrogen. A Ni/TiO₂ cocatalyst with a Ni@TiO₂ core-shell structure was synthesized by Zhang et al. [65] via a modified hydrothermal synthesis method. The MgH₂-Ni/TiO₂ composite with 5 wt% of Ni/TiO₂ allowed a hydrogen absorption of 4.50 wt% to be obtained at 50 °C under an initial hydrogen pressure of 3.0 MPa and a hydrogen desorption of 5.24 wt% in 1800 s at 250 °C under 0.005 MPa of hydrogen pressure [65]. Zhang et al. [66] synthesized and investigated three-dimensional flower-like TiO₂ (fl-TiO₂) and three-dimensional flower-like carbon-wrapped TiO₂ (fl-TiO₂@C) as the catalysts for MgH₂. Both catalysts enhanced the hydrogen sorption kinetics of MgH₂. Superior desorption kinetics of the MgH₂-fl-TiO₂@C composite compared to the MgH₂-fl-TiO₂ composite were observed. The MgH₂-fl-TiO₂@C composite allowed a hydrogen desorption of 6.0 wt% to be obtained in 7 min at 250 °C under a hydrogen pressure of 1 kPa. Concerning the absorption, the MgH₂-fl-TiO₂@C composite showed a hydrogen absorption of 6.3 wt% at 150 °C within 40 min under 5 MPa of hydrogen pressure. Liu et al. [67] synthesized graphene-supported TiO₂ nanoparticles (TiO₂@rGO) using the solvothermal method. It was observed that the MgH₂-TiO₂@rGO composite desorbed 6.0 wt% hydrogen within 6 min at 300 °C and absorbed 5.9 wt% hydrogen within 2 min at 200 °C. The enhancement of the catalytic activity can be due to fine, uniform TiO₂ nanoparticles that were obtained by exploiting the combined effect of ethylene glycol and graphene during the solvothermal process. In addition, rGO can act as an electronic conductive channel to enhance the catalytic effect. Zhang et al. [68] synthesized TiO₂ nanosheets with exposed {001} facets in order to exploit the nanometer-size and highly active {001} facets of anatase TiO₂ to enhance the reaction kinetics of MgH₂. The MgH₂-TiO₂ nanosheet composite allowed a hydrogen desorption of 6.0 wt% to be obtained at 260 °C within 192 s and, in addition, a hydrogen desorption of 1.2 wt% within 300 min at 180 °C was also observed. Furthermore, the composite absorbed 6.1 wt% hydrogen

within 10 s at 150 °C. Also, a hydrogen absorption of 3.3 wt% hydrogen at 50 °C within 10 s was obtained.

The general strategy to improve H₂ storage performance of MgH₂ using TiO₂-based catalysts are reported in Table 2.

Table 2. Summary of strategies adopted to improve H₂ storage performance of MgH₂ using TiO₂-based catalysts.

Composite	Hydrogen Desorption	Hydrogen Desorption Properties (Time, Temp., Pressure)	Hydrogen Absorption	Hydrogen Absorption Properties (Time, Temp., Pressure)	Ref.
MgH ₂ -TiO ₂ /Ti ₃ C ₂ T _x	5.98 wt%	600 s, 300 °C, 0.05 MPa	5.90 wt%	1200 s, 175 °C, 3 MPa	[13]
MgH ₂ -Co/TiO ₂	6.25 wt%	10 min, 265 °C, 0.02 bar	6.07 wt%	10 min, 165 °C, 60 bar	[54]
	6.2 wt%	15 min, 250 °C, 0.02 bar	5.56 wt%	10 min, 130 °C, 60 bar	
	5.4 wt%	100 min, 220 °C, 0.02 bar	4.24 wt%	10 min, 100 °C, 60 bar	
	4.6 wt%	100 min, 210 °C, 0.02 bar	~ 1 wt%	10 min, 50 °C, 60 bar	
MgH ₂ -Ti ₃ C ₂ /TiO ₂ (A)-C	5 wt%	1700 s, 250 °C, 0.05 MPa	4 wt%	800 s, 125 °C, 3 MPa	[55]
MgH ₂ -3DOM TiO ₂	5.75 wt%	1000 s, 300 °C, 0.005 MPa	4.17 wt%	1800 s, 100 °C, 3 MPa	[56]
	5.74 wt%	3000 s, 275 °C, 0.005 MPa	5.40 wt%	1000 s, 175 °C, 3 MPa	
MgH ₂ -TiO ₂ @C	6.5 wt%	7 min, 300 °C, -	6.6 wt%	10 min, 140 °C, 50 bar	[63]
MgH ₂ -TiO ₂ nanorods	~5.5 wt%	5 min, 350 °C, 0.1 bar	5.5 wt%	10 min, 350 °C, 10 bar	[64]
MgH ₂ -Ni/TiO ₂	5.24 wt%	1800 s, 250 °C, 0.005 MPa	4.50 wt%	120 min, 50 °C, 3.0 MPa	[65]
	6.08 wt%	600 s, 300 °C, 0.005 MPa			
MgH ₂ -fl-TiO ₂ @C	6.0 wt%	7 min, 250 °C, 1 kPa	6.3 wt%	40 min, 150 °C, 5 MPa	[66]
	4.9 wt%	60 min, 225 °C, 1 kPa	5.0 wt%	40 min, 100 °C, 5 MPa	
	3.0 wt%	100 min, 200 °C, 1 kPa	3.9 wt%	40 min, 50 °C, 5 MPa	
MgH ₂ -fl-TiO ₂	6.0 wt%	8 min, 250 °C, 1 kPa	6.0 wt%	40 min, 150 °C, 5 MPa	[66]
	3.9 wt%	60 min, 225 °C, 1 kPa			
	0.9 wt%	100 min, 200 °C, 1 kPa			
MgH ₂ -TiO ₂ @rGO	6.0 wt%	6 min, 300 °C, 0.0004 MPa	5.9 wt%	2 min, 200 °C, 3 MPa	[67]
MgH ₂ -TiO ₂ nanosheets	6.0 wt%	192 s, 260 °C, 1 kPa	6.1 wt%	10 s, 150 °C, 5 MPa	[68]
	1.2 wt%	300 min, 180 °C, 1 kPa	3.3 wt%	10 s, 50 °C, 5 MPa	

3. Conclusions

This review has predominantly focused on the utilization of titanium dioxide (TiO₂) in the dual capacity of hydrogen (H₂) production and H₂ storage. Concerning the aspect of H₂ production, extensive efforts have been dedicated to enhancing the photocatalytic efficiency of TiO₂ under both visible and solar light, all while abstaining from the utilization of precious metals. In the realm of solar-driven H₂ production, TiO₂ has frequently undergone modifications involving non-precious metals and metal oxides. Glycerol has consistently featured as the sacrificial agent in the majority of the documented research endeavors.

In the context of visible-light-driven H₂ production, the strategies have commonly entailed the amalgamation of TiO₂ with MoS₂, complemented by the incorporation of a photosensitizer, and the fusion of TiO₂ with CdS. Turning our attention to the subject of H₂ storage, this review has unequivocally demonstrated the catalytic prowess of TiO₂ in augmenting the H₂ storage performance of magnesium hydride (MgH₂). A myriad of strategies has been employed, encompassing the synthesis of TiO₂ nanosheets, flower-like TiO₂ structures, TiO₂ nanorods, TiO₂ nanoparticles, TiO₂/Ti₃C₂T_x heterostructures, graphene-supported TiO₂ nanoparticles, carbon-enveloped nanocrystalline TiO₂, Co/TiO₂ nanocomposites, and Ni@TiO₂ core-shell structures.

The integration of MgH₂ with TiO₂-based catalysts has yielded notable enhancements in H₂ absorption and desorption kinetics, leading to lower operating temperatures for H₂ desorption and absorption processes, especially when compared to pure MgH₂.

Author Contributions: Conceptualization, V.D.M. and M.C.; writing—original draft preparation, A.D.B.; writing—review and editing A.D.L., P.P., R.R., V.D.M. and M.C.; supervision, V.D.M. and M.C. All authors have read and agreed to the published version of the manuscript.

Funding: M.C. kindly acknowledges PRP@CERIC-CUP J97G22000400006 for sponsoring her salary and work. V.D.M. kindly acknowledges Programma Operativo Nazionale (PON) Ricerca e Innovazione 2014–2020-Azione IV.6 “Contratti su tematiche green”-DM 1062/2021 for sponsoring her salary and work. A.D.L. acknowledges PON 2014-2020, Asse I “Capitale Umano”, “Dottorati Innovativi con caratterizzazione industriale”, CUP F85F21005780001; and A.D.B. kindly acknowledges Progetto Tisma, CUP F83C21000150001 PNR–MUR. M4C2–Dalla ricerca all’impresa—1.1: Fondo per il Programma Nazionale della Ricerca (PNR) e Progetti di Ricerca di Rilevante Interesse Nazionale (PRIN).

Institutional Review Board Statement: Not applicable.

Informed Consent Statement: Not applicable.

Data Availability Statement: Not applicable.

Conflicts of Interest: The authors declare no conflict of interest.

References

1. Police, A.K.R.; Vattikuti, S.V.P.; Mandari, K.K.; Chennaiahgari, M.; Sharma, P.; Valluri, D.K.; Byon, C. Bismuth oxide cocatalyst and copper oxide sensitizer in $\text{Cu}_2\text{O}/\text{TiO}_2/\text{Bi}_2\text{O}_3$ ternary photocatalyst for efficient hydrogen production under solar light irradiation. *Ceram. Int.* **2018**, *44*, 11783–11791. [[CrossRef](#)]
2. Huang, J.-F.; Lei, Y.; Luo, T.; Liu, J.-M. Photocatalytic H_2 Production from Water by Metal-free Dye-sensitized TiO_2 Semiconductors: The Role and Development Process of Organic Sensitizers. *ChemSusChem* **2020**, *13*, 5863–5895. [[CrossRef](#)] [[PubMed](#)]
3. Singh, R.; Dutta, S. A review on H_2 production through photocatalytic reactions using $\text{TiO}_2/\text{TiO}_2$ -assisted catalysts. *Fuel* **2018**, *220*, 607–620. [[CrossRef](#)]
4. Ge, M.; Cai, J.; Iocozzia, J.; Cao, C.; Huang, J.; Zhang, X.; Shen, J.; Wang, S.; Zhang, S.; Zhang, K.-Q.; et al. A review of TiO_2 nanostructured catalysts for sustainable H_2 generation. *Int. J. Hydrogen Energy* **2017**, *42*, 8418–8449. [[CrossRef](#)]
5. Cai, J.; Shen, J.; Zhang, X.; Ng, Y.H.; Huang, J.; Guo, W.; Lin, C.; Lai, Y. Light-Driven Sustainable Hydrogen Production Utilizing TiO_2 Nanostructures: A Review. *Small Methods* **2019**, *3*, 1800184. [[CrossRef](#)]
6. Abe, R. Recent progress on photocatalytic and photoelectrochemical water splitting under visible light irradiation. *J. Photochem. Photobiol. C Photochem. Rev.* **2010**, *11*, 179–209. [[CrossRef](#)]
7. Fajrina, N.; Tahir, M. A critical review in strategies to improve photocatalytic water splitting towards hydrogen production. *Int. J. Hydrogen Energy* **2019**, *44*, 540–577. [[CrossRef](#)]
8. De Matteis, V.; Cannavale, A.; Blasi, L.; Quarta, A.; Gigli, G. Chromogenic device for cystic fibrosis precocious diagnosis: A “Point of Care” tool for sweat test. *Sens. Actuators B Chem.* **2016**, *225*, 474–480. [[CrossRef](#)]
9. Wondimu, T.H.; Bayeh, A.W.; Kabtamu, D.M.; Xu, Q.; Leung, P.; Shah, A.A. Recent progress on tungsten oxide-based materials for the hydrogen and oxygen evolution reactions. *Int. J. Hydrogen Energy* **2022**, *47*, 20378–20397. [[CrossRef](#)]
10. Yuan, Y.; Lu, H.; Ji, Z.; Zhong, J.; Ding, M.; Chen, D.; Li, Y.; Tu, W.; Cao, D.; Yu, Z.; et al. Enhanced visible-light-induced hydrogen evolution from water in a noble-metal-free system catalyzed by $\text{ZnTCPP-MoS}_2/\text{TiO}_2$ assembly. *Chem. Eng. J.* **2015**, *275*, 8–16. [[CrossRef](#)]
11. Díaz, L.; Rodríguez, V.D.; González-Rodríguez, M.; Rodríguez-Castellón, E.; Algarra, M.; Núñez, P.; Moretti, E. M/ TiO_2 (M = Fe, Co, Ni, Cu, Zn) catalysts for photocatalytic hydrogen production under UV and visible light irradiation. *Inorg. Chem. Front.* **2021**, *8*, 3491–3500. [[CrossRef](#)]
12. Yang, Y.; Gao, P.; Wang, Y.; Sha, L.; Ren, X.; Zhang, J.; Yang, P.; Wu, T.; Chen, Y.; Li, X. A simple and efficient hydrogen production-storage hybrid system (Co/ TiO_2) for synchronized hydrogen photogeneration with uptake. *J. Mater. Chem. A* **2017**, *5*, 9198–9203. [[CrossRef](#)]
13. Gao, H.; Shi, R.; Shao, Y.; Liu, Y.; Zhu, Y.; Zhang, J.; Hu, X.; Li, L.; Ba, Z. One-step self-assembly of $\text{TiO}_2/\text{MXene}$ heterostructures for improving the hydrogen storage performance of magnesium hydride. *J. Alloys Compd.* **2022**, *895*, 162635. [[CrossRef](#)]
14. Liang, G.; Huot, J.; Boily, S.; Van Neste, A.; Schulz, R. Catalytic effect of transition metals on hydrogen sorption in nanocrystalline ball milled MgH_2 -Tm (Tm=Ti, V, Mn, Fe and Ni) systems. *J. Alloys Compd.* **1999**, *292*, 247–252. [[CrossRef](#)]
15. Chen, G.; Zhang, Y.; Chen, J.; Guo, X.; Zhu, Y.; Li, L. Enhancing hydrogen storage performances of MgH_2 by Ni nano-particles over mesoporous carbon CMK-3. *Nanotechnology* **2018**, *29*, 265705. [[CrossRef](#)]
16. Sadhasivam, T.; Sterlin Leo Hudson, M.; Pandey, S.K.; Bhatnagar, A.; Singh, M.K.; Gurunathan, K.; Srivastava, O.N. Effects of nano size mischmetal and its oxide on improving the hydrogen sorption behaviour of MgH_2 . *Int. J. Hydrogen Energy* **2013**, *38*, 7353–7362. [[CrossRef](#)]

17. Zhang, X.; Shen, Z.; Jian, N.; Hu, J.; Du, F.; Yao, J.; Gao, M.; Liu, Y.; Pan, H. A novel complex oxide $\text{TiVO}_{3.5}$ as a highly active catalytic precursor for improving the hydrogen storage properties of MgH_2 . *Int. J. Hydrogen Energy* **2018**, *43*, 23327–23335. [[CrossRef](#)]
18. Patah, A.; Takasaki, A.; Szymid, J.S. Influence of multiple oxide ($\text{Cr}_2\text{O}_3/\text{Nb}_2\text{O}_5$) addition on the sorption kinetics of MgH_2 . *Int. J. Hydrogen Energy* **2009**, *34*, 3032–3037. [[CrossRef](#)]
19. Bhat, V.V.; Rougier, A.; Aymard, L.; Darok, X.; Nazri, G.; Tarascon, J.M. Catalytic activity of oxides and halides on hydrogen storage of MgH_2 . *J. Power Sources* **2006**, *159*, 107–110. [[CrossRef](#)]
20. Wang, P.; Tian, Z.; Wang, Z.; Xia, C.; Yang, T.; Ou, X. Improved hydrogen storage properties of MgH_2 using transition metal sulfides as catalyst. *Int. J. Hydrogen Energy* **2021**, *46*, 27107–27118. [[CrossRef](#)]
21. Zhang, W.; Xu, G.; Cheng, Y.; Chen, L.; Huo, Q.; Liu, S. Improved hydrogen storage properties of MgH_2 by the addition of FeS_2 micro-spheres. *Dalton Trans.* **2018**, *47*, 5217–5225. [[CrossRef](#)]
22. Plerdsranoy, P.; Thiangviriyaya, S.; Dansirima, P.; Thongtan, P.; Kaewsuwan, D.; Chanlek, N.; Utke, R. Synergistic effects of transition metal halides and activated carbon nanofibers on kinetics and reversibility of MgH_2 . *J. Phys. Chem. Solids* **2019**, *124*, 81–88. [[CrossRef](#)]
23. Pelaez, M.; Nolan, N.T.; Pillai, S.C.; Seery, M.K.; Falaras, P.; Kontos, A.G.; Dunlop, P.S.M.; Hamilton, J.W.J.; Byrne, J.A.; O’Shea, K.; et al. A review on the visible light active titanium dioxide photocatalysts for environmental applications. *Appl. Catal. B Environ.* **2012**, *125*, 331–349. [[CrossRef](#)]
24. Carp, O.; Huisman, C.L.; Reller, A. Photoinduced reactivity of titanium dioxide. *Prog. Solid State Chem.* **2004**, *32*, 33–177. [[CrossRef](#)]
25. Haggerty, J.E.S.; Schelhas, L.T.; Kitchaev, D.A.; Mangum, J.S.; Garten, L.M.; Sun, W.; Stone, K.H.; Perkins, J.D.; Toney, M.F.; Ceder, G.; et al. High-fraction brookite films from amorphous precursors. *Sci. Rep.* **2017**, *7*, 15232. [[CrossRef](#)]
26. Li, G.; Chen, L.; Graham, M.E.; Gray, K.A. A comparison of mixed phase titania photocatalysts prepared by physical and chemical methods: The importance of the solid–solid interface. *J. Mol. Catal. Chem.* **2007**, *275*, 30–35. [[CrossRef](#)]
27. Zhang, J.; Zhou, P.; Liu, J.; Yu, J. New understanding of the difference of photocatalytic activity among anatase, rutile and brookite TiO_2 . *Phys. Chem. Chem. Phys.* **2014**, *16*, 20382–20386. [[CrossRef](#)]
28. Kang, X.; Liu, S.; Dai, Z.; He, Y.; Song, X.; Tan, Z. Titanium Dioxide: From Engineering to Applications. *Catalysts* **2019**, *9*, 191. [[CrossRef](#)]
29. Chen, X.; Shen, S.; Guo, L.; Mao, S.S. Semiconductor-based Photocatalytic Hydrogen Generation. *Chem. Rev.* **2010**, *110*, 6503–6570. [[CrossRef](#)]
30. Serafin, J.; Ouzzine, M.; Sreńscek-Nazzal, J.; Llorca, J. Photocatalytic hydrogen production from alcohol aqueous solutions over TiO_2 -activated carbon composites decorated with Au and Pt. *J. Photochem. Photobiol. Chem.* **2022**, *425*, 113726. [[CrossRef](#)]
31. Dang, H.; Cheng, Z.; Yang, W.; Chen, W.; Huang, W.; Li, B.; Shi, Z.; Qiu, Y.; Dong, X.; Fan, H. Room-temperature synthesis of Cu_xS ($x = 1$ or 2) co-modified TiO_2 nanocomposite and its highly efficient photocatalytic H_2 production activity. *J. Alloys Compd.* **2017**, *709*, 422–430. [[CrossRef](#)]
32. Jovic, V.; Al-Azri, Z.H.N.; Chen, W.-T.; Sun-Waterhouse, D.; Idriss, H.; Waterhouse, G.I.N. Photocatalytic H_2 Production from Ethanol–Water Mixtures Over Pt/ TiO_2 and Au/ TiO_2 Photocatalysts: A Comparative Study. *Top. Catal.* **2013**, *56*, 1139–1151. [[CrossRef](#)]
33. Jovic, V.; Chen, W.-T.; Sun-Waterhouse, D.; Blackford, M.G.; Idriss, H.; Waterhouse, G.I.N. Effect of gold loading and TiO_2 support composition on the activity of Au/ TiO_2 photocatalysts for H_2 production from ethanol–water mixtures. *J. Catal.* **2013**, *305*, 307–317. [[CrossRef](#)]
34. Serafin, J.; Soler, L.; Vega, D.; Rodríguez, Á.; Llorca, J. Macroporous silicon coated with M/ TiO_2 ($M = \text{Au}, \text{Pt}$) as a highly efficient photoreactor for hydrogen production. *Chem. Eng. J.* **2020**, *393*, 124701. [[CrossRef](#)]
35. Rusinque, B.; Escobedo, S.; de Lasa, H. Photoreduction of a Pd-Doped Mesoporous TiO_2 Photocatalyst for Hydrogen Production under Visible Light. *Catalysts* **2020**, *10*, 74. [[CrossRef](#)]
36. Sadanandam, G.; Lalitha, K.; Kumari, V.D.; Shankar, M.V.; Subrahmanyam, M. Cobalt doped TiO_2 : A stable and efficient photocatalyst for continuous hydrogen production from glycerol: Water mixtures under solar light irradiation. *Int. J. Hydrogen Energy* **2013**, *38*, 9655–9664. [[CrossRef](#)]
37. Yan, Z.; Yu, X.; Zhang, Y.; Jia, H.; Sun, Z.; Du, P. Enhanced visible light-driven hydrogen production from water by a noble-metal-free system containing organic dye-sensitized titanium dioxide loaded with nickel hydroxide as the cocatalyst. *Appl. Catal. B Environ.* **2014**, *160–161*, 173–178. [[CrossRef](#)]
38. Subha, N.; Mahalakshmi, M.; Myilsamy, M.; Neppolian, B.; Murugesan, V. Direct Z-scheme heterojunction nanocomposite for the enhanced solar H_2 production. *Appl. Catal. Gen.* **2018**, *553*, 43–51. [[CrossRef](#)]
39. Kotesch Kumar, M.; Naresh, G.; Vijay Kumar, V.; Sai Vasista, B.; Sasikumar, B.; Venugopal, A. Improved H_2 yields over Cu-Ni- TiO_2 under solar light irradiation: Behaviour of alloy nano particles on photocatalytic H_2O splitting. *Appl. Catal. B Environ.* **2021**, *299*, 120654. [[CrossRef](#)]
40. Reddy, J.K.; Lalitha, K.; Reddy, P.V.L.; Sadanandam, G.; Subrahmanyam, M.; Kumari, V.D. Fe/ TiO_2 : A Visible Light Active Photocatalyst for the Continuous Production of Hydrogen from Water Splitting Under Solar Irradiation. *Catal. Lett.* **2014**, *144*, 340–346. [[CrossRef](#)]

41. Subha, N.; Mahalakshmi, M.; Myilsamy, M.; Lakshmana Reddy, N.; Shankar, M.V.; Neppolian, B.; Murugesan, V. Effective excitons separation on graphene supported ZrO₂-TiO₂ heterojunction for enhanced H₂ production under solar light. *Int. J. Hydrogen Energy* **2018**, *43*, 3905–3919. [[CrossRef](#)]
42. Praveen Kumar, D.; Shankar, M.V.; Mamatha Kumari, M.; Sadanandam, G.; Srinivas, B.; Durgakumari, V. Nano-size effects on CuO/TiO₂ catalysts for highly efficient H₂ production under solar light irradiation. *Chem. Commun.* **2013**, *49*, 9443. [[CrossRef](#)] [[PubMed](#)]
43. Subha, N.; Mahalakshmi, M.; Monika, S.; Neppolian, B. Ni(OH)₂-Cu_xO-TiO₂ nanocomposite for the enhanced H₂ production under solar light: The mechanistic pathway. *Int. J. Hydrogen Energy* **2020**, *45*, 7552–7561. [[CrossRef](#)]
44. Gao, B.; Yuan, X.; Lu, P.; Lin, B.; Chen, Y. Enhanced visible-light-driven photocatalytic H₂-production activity of CdS-loaded TiO₂ microspheres with exposed (001) facets. *J. Phys. Chem. Solids* **2015**, *87*, 171–176. [[CrossRef](#)]
45. Qian, Y.; Yang, M.; Zhang, F.; Du, J.; Li, K.; Lin, X.; Zhu, X.; Lu, Y.; Wang, W.; Kang, D.J. A stable and highly efficient visible-light-driven hydrogen evolution porous CdS/WO₃/TiO₂ photocatalysts. *Mater. Charact.* **2018**, *142*, 43–49. [[CrossRef](#)]
46. Luo, X.; Ke, Y.; Yu, L.; Wang, Y.; Homewood, K.P.; Chen, X.; Gao, Y. Tandem CdS/TiO₂(B) nanosheet photocatalysts for enhanced H₂ evolution. *Appl. Surf. Sci.* **2020**, *515*, 145970. [[CrossRef](#)]
47. Zhu, Y.; Wang, Y.; Chen, Z.; Qin, L.; Yang, L.; Zhu, L.; Tang, P.; Gao, T.; Huang, Y.; Sha, Z.; et al. Visible light induced photocatalysis on CdS quantum dots decorated TiO₂ nanotube arrays. *Appl. Catal. Gen.* **2015**, *498*, 159–166. [[CrossRef](#)]
48. Shah, S.A.; Khan, I.; Yuan, A. MoS₂ as a Co-Catalyst for Photocatalytic Hydrogen Production: A Mini Review. *Molecules* **2022**, *27*, 3289. [[CrossRef](#)]
49. Yuan, Y.-J.; Fang, G.; Chen, D.; Huang, Y.; Yang, L.-X.; Cao, D.-P.; Wang, J.; Yu, Z.-T.; Zou, Z.-G. High light harvesting efficiency CuInS₂ quantum dots/TiO₂/MoS₂ photocatalysts for enhanced visible light photocatalytic H₂ production. *Dalton Trans.* **2018**, *47*, 5652–5659. [[CrossRef](#)]
50. Shen, M.; Yan, Z.; Yang, L.; Du, P.; Zhang, J.; Xiang, B. MoS₂ nanosheet/TiO₂ nanowire hybrid nanostructures for enhanced visible-light photocatalytic activities. *Chem. Commun* **2014**, *50*, 15447–15449. [[CrossRef](#)]
51. Ma, B.; Guan, P.-Y.; Li, Q.-Y.; Zhang, M.; Zang, S.-Q. MOF-Derived Flower-like MoS₂@TiO₂ Nanohybrids with Enhanced Activity for Hydrogen Evolution. *ACS Appl. Mater. Interfaces* **2016**, *8*, 26794–26800. [[CrossRef](#)] [[PubMed](#)]
52. Du, J.; Wang, H.; Yang, M.; Zhang, F.; Wu, H.; Cheng, X.; Yuan, S.; Zhang, B.; Li, K.; Wang, Y.; et al. Highly efficient hydrogen evolution catalysis based on MoS₂/CdS/TiO₂ porous composites. *Int. J. Hydrogen Energy* **2018**, *43*, 9307–9315. [[CrossRef](#)]
53. Qin, N.; Xiong, J.; Liang, R.; Liu, Y.; Zhang, S.; Li, Y.; Li, Z.; Wu, L. Highly efficient photocatalytic H₂ evolution over MoS₂/CdS-TiO₂ nanofibers prepared by an electrospinning mediated photodeposition method. *Appl. Catal. B Environ.* **2017**, *202*, 374–380. [[CrossRef](#)]
54. Chen, M.; Xiao, X.; Zhang, M.; Zheng, J.; Liu, M.; Wang, X.; Jiang, L.; Chen, L. Highly dispersed metal nanoparticles on TiO₂ acted as nano redox reactor and its synergistic catalysis on the hydrogen storage properties of magnesium hydride. *Int. J. Hydrogen Energy* **2019**, *44*, 15100–15109. [[CrossRef](#)]
55. Gao, H.; Liu, Y.; Zhu, Y.; Zhang, J.; Li, L. Catalytic effect of sandwich-like Ti₃C₂/TiO₂(A)-C on hydrogen storage performance of MgH₂. *Nanotechnology* **2020**, *31*, 115404. [[CrossRef](#)] [[PubMed](#)]
56. Shao, Y.; Gao, H.; Tang, Q.; Liu, Y.; Liu, J.; Zhu, Y.; Zhang, J.; Li, L.; Hu, X.; Ba, Z. Ultra-fine TiO₂ nanoparticles supported on three-dimensionally ordered macroporous structure for improving the hydrogen storage performance of MgH₂. *Appl. Surf. Sci.* **2022**, *585*, 152561. [[CrossRef](#)]
57. Huang, Y.; Shao, H.; Zhang, Q.; Zang, L.; Guo, H.; Liu, Y.; Jiao, L.; Yuan, H.; Wang, Y. Layer-by-layer uniformly confined Graphene-NaAlH₄ composites and hydrogen storage performance. *Int. J. Hydrogen Energy* **2020**, *45*, 28116–28122. [[CrossRef](#)]
58. Ma, Z.; Liu, J.; Zhao, Y.; Zhang, J.; Zhu, Y.; Zhang, Y.; Liu, Y.; Li, L. Enhanced dehydrogenation properties of LiAlH₄-Mg₂NiH₄ nanocomposites via doping Ti-based catalysts. *Mater. Res. Express* **2019**, *6*, 075067. [[CrossRef](#)]
59. Saldan, I.; Campesi, R.; Zavorotynska, O.; Spoto, G.; Baricco, M.; Arendarska, A.; Taube, K.; Dornheim, M. Enhanced hydrogen uptake/release in 2LiH-MgB₂ composite with titanium additives. *Int. J. Hydrogen Energy* **2012**, *37*, 1604–1612. [[CrossRef](#)]
60. Xian, K.; Nie, B.; Li, Z.; Gao, M.; Li, Z.; Shang, C.; Liu, Y.; Guo, Z.; Pan, H. TiO₂ decorated porous carbonaceous network structures offer confinement, catalysis and thermal conductivity for effective hydrogen storage of LiBH₄. *Chem. Eng. J.* **2021**, *407*, 127156. [[CrossRef](#)]
61. Rafi-ud-din; Xuanhui, Q.; Zahid, G.H.; Asghar, Z.; Shahzad, M.; Iqbal, M.; Ahmad, E. Improved hydrogen storage performances of MgH₂-NaAlH₄ system catalyzed by TiO₂ nanoparticles. *J. Alloys Compd.* **2014**, *604*, 317–324. [[CrossRef](#)]
62. Guo, L.; Jiao, L.; Li, L.; Wang, Q.; Liu, G.; Du, H.; Wu, Q.; Du, J.; Yang, J.; Yan, C.; et al. Enhanced desorption properties of LiBH₄ incorporated into mesoporous TiO₂. *Int. J. Hydrogen Energy* **2013**, *38*, 162–168. [[CrossRef](#)]
63. Zhang, X.; Leng, Z.; Gao, M.; Hu, J.; Du, F.; Yao, J.; Pan, H.; Liu, Y. Enhanced hydrogen storage properties of MgH₂ catalyzed with carbon-supported nanocrystalline TiO₂. *J. Power Sources* **2018**, *398*, 183–192. [[CrossRef](#)]
64. Jardim, P.M.; da Conceição, M.O.T.; Brum, M.C.; dos Santos, D.S. Hydrogen sorption kinetics of ball-milled MgH₂-TiO₂ based 1D nanomaterials with different morphologies. *Int. J. Hydrogen Energy* **2015**, *40*, 17110–17117. [[CrossRef](#)]
65. Zhang, J.; Shi, R.; Zhu, Y.; Liu, Y.; Zhang, Y.; Li, S.; Li, L. Remarkable Synergistic Catalysis of Ni-Doped Ultrafine TiO₂ on Hydrogen Sorption Kinetics of MgH₂. *ACS Appl. Mater. Interfaces* **2018**, *10*, 24975–24980. [[CrossRef](#)]
66. Zhang, M.; Xiao, X.; Luo, B.; Liu, M.; Chen, M.; Chen, L. Superior de/hydrogenation performances of MgH₂ catalyzed by 3D flower-like TiO₂@C nanostructures. *J. Energy Chem.* **2020**, *46*, 191–198. [[CrossRef](#)]

67. Liu, G.; Wang, L.; Hu, Y.; Sun, C.; Leng, H.; Li, Q.; Wu, C. Enhanced catalytic effect of TiO₂@rGO synthesized by one-pot ethylene glycol-assisted solvothermal method for MgH₂. *J. Alloys Compd.* **2021**, *881*, 160644. [[CrossRef](#)]
68. Zhang, M.; Xiao, X.; Wang, X.; Chen, M.; Lu, Y.; Liu, M.; Chen, L. Excellent catalysis of TiO₂ nanosheets with high-surface-energy {001} facets on the hydrogen storage properties of MgH₂. *Nanoscale* **2019**, *11*, 7465–7473. [[CrossRef](#)]
69. Xiong, R.; Sang, G.; Yan, X.; Zhang, G.; Ye, X.; Zhu, X. Direct synthesis of nanocrystalline titanium dioxide/carbon composite and its catalytic effect on NaAlH₄ for hydrogen storage. *Int. J. Hydrogen Energy* **2011**, *36*, 15652–15657. [[CrossRef](#)]
70. Xiong, R.; Sang, G.; Yan, X.; Zhang, G.; Ye, X.; Jiang, C.; Luo, L. Improvement of the hydrogen storage kinetics of NaAlH₄ with nanocrystalline titanium dioxide loaded carbon spheres (Ti-CSs) by melt infiltration. *Int. J. Hydrogen Energy* **2012**, *37*, 10222–10228. [[CrossRef](#)]
71. Zhao, Y.; Han, M.; Wang, H.; Chen, C.; Chen, J. LiAlH₄ supported on TiO₂/hierarchically porous carbon nanocomposites with enhanced hydrogen storage properties. *Inorg. Chem. Front.* **2016**, *3*, 1536–1542. [[CrossRef](#)]
72. Amama, P.B.; Grant, J.T.; Shamberger, P.J.; Voevodin, A.A.; Fisher, T.S. Improved Dehydrogenation Properties of Ti-Doped LiAlH₄: Role of Ti Precursors. *J. Phys. Chem. C* **2012**, *116*, 21886–21894. [[CrossRef](#)]
73. Mustafa, N.S.; Yahya, M.S.; Itam Sulaiman, N.N.; Abdul Halim Yap, M.F.A.; Ismail, M. Enhanced the hydrogen storage properties and reaction mechanisms of 4MgH₂ + LiAlH₄ composite system by addition with TiO₂. *Int. J. Energy Res.* **2021**, *45*, 21365–21374. [[CrossRef](#)]

Disclaimer/Publisher's Note: The statements, opinions and data contained in all publications are solely those of the individual author(s) and contributor(s) and not of MDPI and/or the editor(s). MDPI and/or the editor(s) disclaim responsibility for any injury to people or property resulting from any ideas, methods, instructions or products referred to in the content.